Chapter 2
Analysis of Autonomous Many-Body Particle Models from Geometric Perspective and Its Applications

Satoshi Tsujimoto, Tsuyoshi Kato, Ryosuke Kojima, Kazuki Maeda, and Francesco Zanlungo

2.1 Introduction

Autonomous many-body particle systems, such as traffic flow models, pedestrian flow models, and molecular biology models, are very important targets that appear in various fields. Since the behavior of these systems is essentially nonlinear and is rich in variety and flexibility, it is important to grasp the whole picture of the system not only numerically, but also through theoretical analysis.

For interacting systems of many-body particles, we have been studying

A. the development of analytical methods,
B. the investigation and extension of fundamental models.

For A., we have mainly worked on the following analytical methods from the viewpoint of geometry: (i) derivation and analysis of the Burgers cellular automaton

S. Tsujimoto (✉)
Graduate School of Informatics, Kyoto University, Yoshida-honmachi, Sakyo-ku, Kyoto 606-8501, Japan
e-mail: tsujimoto.satoshi.5s@kyoto-u.ac.jp

T. Kato
Kyoto University, Kitashirakawa Oiwake-cho, Sakyo-ku, Kyoto 606-8502, Japan
e-mail: kato.tsuyoshi.5m@kyoto-u.ac.jp

R. Kojima
Kyoto University, 53 Kawahara-cho, Shogoin, Sakyo-ku, Kyoto 606-8507, Japan
e-mail: kojima.ryosuke.8e@kyoto-u.ac.jp

K. Maeda
The University of Fukuchiyama, 3370 Hori, Fukuchiyama, Kyoto 620-0886, Japan
e-mail: kmaeda@kmaeda.net

F. Zanlungo
International Professional University of Technology in Osaka, 3-3-1 Umeda, Kita-ku, Osaka 530-0001, Japan
e-mail: zanlungo@atr.jp

(BCA) and the box-ball system (BBS) by the methods of tropical geometry and ultra-discrete systems, (ii) various studies on many-body particle interaction systems based on discrete Morse theory from a phase-geometric approach, and (iii) development of a fundamental model for B., which is a model of many-body particle interaction systems. As primary models to be treated in B., there are various models such as traffic flow, pedestrian flow, and molecular biology models. In this paper, we will mainly focus on BCA, BBS, and the totally asymmetric simple exclusion process (TASEP), which will be briefly introduced in this paper. The method of tropical geometry is effective not only in analytical methods but also in the derivation of new models. In the modeling of particle systems, there are examples of successful extraction of the skeletal part in particular, and the BBS obtained from the Korteweg-de Vries (KdV) equation and its ultra-discretization of the nonlinear partial differential equation is well known. Although research results from this perspective are not yet at the level of basic theory, it is possible to investigate various extensions of cellular automata and analytical solutions to their initial value problems. As an unexpected byproduct of the above research, we were also able to clarify the relationship between the BBS and a computational procedure for invariant factors of integer matrices.

In Sect. 2.2, we outline the discrete Morse theory methods used. Section 2.3 gives an example of the application of the discrete Morse theory method to traffic flow model analysis. In Sect. 2.4, we derive a model with more general degrees of freedom by adding internal degrees of freedom, such as explicit and implicit degrees of freedom, to the particle system, and we also derive a quantum version of TASEP and discuss its results. Finally, in Sect. 2.5, we will discuss pedestrian flow models as the next subject and summarize the current status and future prospects.

2.2 Discrete Morse Theory

In this section, we give a brief introduction to topology, especially homology, Morse theory, and discrete Morse theory.

2.2.1 Homology

The homology theory is a fundamental tool to study differentiable manifolds viewed as topological spaces. Homology groups $H_k(M)$, $k = 0, 1, 2, \ldots$, of a manifold M are abelian groups that represent topological invariants of M; i.e. two manifolds have the isomorphic homology groups if they can be continuously deformed into each other (homotopy equivalent; note that the reverse is not always true). In the simplest case, the kth homology group $H_k(M)$ becomes $\mathbb{Z}^n$ that means

- the case of $k = 0$: the number of connected components in M is n;
- the case of $k \geq 1$: roughly, the number of k-dimensional holes in M is n,

$$
\begin{array}{llll}
\text{(a)} & \text{(b)} & \text{(c)} & \text{(d)}
\end{array}
$$

<table>
<tr><td>(a)</td><td>(b)</td><td>(c)</td><td>(d)</td></tr>
</table>

h.e.~

<table>
<tr>
<td>$H_0 = \mathbb{Z},$
$H_k = 0 \quad$ for $k \geq 1$.</td>
<td>$H_0 = \mathbb{Z},$
$H_1 = \mathbb{Z},$
$H_k = 0 \quad$ for $k \geq 2$.</td>
<td>$H_0 = \mathbb{Z},$
$H_1 = \mathbb{Z},$
$H_k = 0 \quad$ for $k \geq 2$.</td>
<td>$H_0 = \mathbb{Z},$
$H_1 = 0,$
$H_2 = \mathbb{Z},$
$H_k = 0 \quad$ for $k \geq 3$.</td>
</tr>
</table>

Fig. 2.1 Examples of homology groups. **a** A disk has no hole. **b** A circle has a 1-dimensional hole. **c** An annulus also has a 1-dimensional hole. A circle and an annulus are homotopy equivalent. **d** A sphere has a 2-dimensional hole

where n is called the Betti number. Figure 2.1 gives several examples. In more complicated cases, the homology groups may have finite subgroups called torsion subgroups, but we do not explain them here.

If two manifolds have different homology, then they cannot be homotopy equivalent. Hence, the computation of the homology groups of differentiable manifolds is a first step to study topology of manifolds (see, e.g. [15]). There is Morse theory that is useful for the construction of homology groups.

2.2.2 Morse Theory

Let us consider two differentiable functions on a manifold $f, g \colon M \to \mathbb{R}$, where f and g do not have any degenerate critical points. The Morse theory is able to construct the isomorphic homology groups of M from both different functions f and g; i.e. any generic functions on a manifold M reflect the topology of M directly. A "simpler" function that has as few critical points as possible makes it easy to compute homology groups.

We introduce gradient vector fields here. Consider a situation that a local coordinate system with variables $x_1, x_2, \ldots, x_n$ is given on $U \subset M$. A map $\varphi_U \colon U \to \mathbb{R}^n$ represents this coordinate. Then, the tangent space at a point $p \in U$ denoted by $T_p M$ is defined as a linear space formally spanned by the differential operators $\frac{\partial}{\partial x_1}$, $\frac{\partial}{\partial x_2}$, $\ldots$, $\frac{\partial}{\partial x_n}$. The tangent bundle of M is defined by $TM := \sqcup_{p \in M} T_p M$. For the tangent space $T_p M$, we can consider a dual space $T_p^* M$, which is called the cotangent space. The cotangent bundle $T^* M := \sqcup_{p \in M} T_p^* M$ is also defined. There is a basis $\{dx_1, dx_2, \ldots, dx_n\}$ of $T_p^* M$ satisfying

$$dx_i \left(\frac{\partial}{\partial x_j} \right) = \delta_{ij}, \quad i, j = 1, 2, \dots, n,$$

where δ_{ij} is the Kronecker delta.

For a function $f : M \to \mathbb{R}$, the differential 1-form of f at $p \in U$ is defined by

$$df_p := \sum_{i=1}^{n} \frac{\partial (f \circ \varphi_U^{-1})}{\partial x_i} dx_i \in T_p^* M.$$

If a Riemannian metric $g_p \in T_p^* M \otimes T_p^* M$ is given at each point $p \in M$, then the gradient of f denoted by $\nabla f : M \to TM; p \mapsto \nabla f(p) \in T_p M$ is uniquely defined by the equation

$$g_p(\nabla f(p), v_p) = df_p(v_p)$$

for all $p \in M$ and $v_p \in T_p M$. Although this definition may look a bit complicated, this is exactly a generalization of the gradient on the Euclidean space. (Consider the case $g_p = \sum_{i=1}^{n} dx_i \otimes dx_i$ for all $p \in M$. That may be helpful for understanding the meaning.)
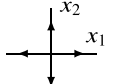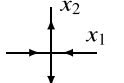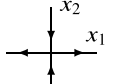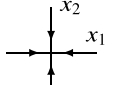
A point $\overline{p} \in M$ is called a critical point of f if $\nabla f(\overline{p}) = 0$. For the Hessian matrix of f at a point p defined by

$$H_f(p) := \begin{pmatrix} \frac{\partial^2 (f \circ \varphi_U^{-1})}{\partial x_1^2} & \frac{\partial^2 (f \circ \varphi_U^{-1})}{\partial x_1 \partial x_2} & \cdots & \frac{\partial^2 (f \circ \varphi_U^{-1})}{\partial x_1 \partial x_n} \\ \frac{\partial^2 (f \circ \varphi_U^{-1})}{\partial x_2 \partial x_1} & \frac{\partial^2 (f \circ \varphi_U^{-1})}{\partial x_2^2} & \cdots & \frac{\partial^2 (f \circ \varphi_U^{-1})}{\partial x_2 \partial x_n} \\ \vdots & \vdots & \ddots & \vdots \\ \frac{\partial^2 (f \circ \varphi_U^{-1})}{\partial x_n \partial x_1} & \frac{\partial^2 (f \circ \varphi_U^{-1})}{\partial x_n \partial x_2} & \cdots & \frac{\partial^2 (f \circ \varphi_U^{-1})}{\partial x_n^2} \end{pmatrix} (\varphi_U(p)),$$

if $\det H_f(\overline{p}) \neq 0$ then $\overline{p}$ is called a non-degenerate critical point. If all the critical points of f are non-degenerate then f is called a Morse function. It is known that Morse functions are generic in the set of smooth functions. The index of a critical point $\overline{p}$ of f, denoted by λ in this section, is defined as the number of the negative eigenvalues of the Hessian matrix $H_f(\overline{p})$. Table 2.1 shows examples of critical points and their indices. We can see that critical points of index 0, 1, and 2 in the two-dimensional Euclidean space correspond to local minimum points, saddle points, and local maximum points, respectively. In the examples, we consider critical points on the Euclidean space, but we also can consider critical points on any manifolds in general. See Fig. 2.2.

From critical points and a gradient vector field, we can compute homology groups (called Morse homology) of M. Let p and q be critical points and $\mathcal{M}(p, q)$ be the set of all the integral curves of $-\nabla f$ from p to q; i.e. $\gamma \in \mathcal{M}(p, q)$ means $\frac{d\gamma}{dt}(t) = -\nabla f(\gamma(t))$, $\lim_{t \to -\infty} = p$ and $\lim_{t \to +\infty} = q$. For example, in Fig. 2.2, $\mathcal{M}(p_3, p_2)$ has two integral curves γ_1 and γ_2, and $\gamma_1 - \gamma_2$ makes a cycle. We give a

Table 2.1 Examples of critical points (the origin in these cases) and their indices λ on the two-dimensional Euclidean space

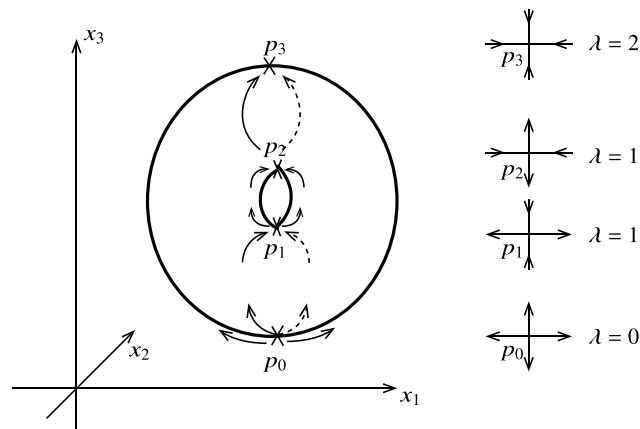| $f \circ \varphi_U^{-1}(x_1, x_2)$	∇f	gradient at the origin	λ
$x_1^2 + x_2^2$	$2x_1 \dfrac{\partial}{\partial x_1} + 2x_2 \dfrac{\partial}{\partial x_2}$		0
$-x_1^2 + x_2^2$	$-2x_1 \dfrac{\partial}{\partial x_1} + 2x_2 \dfrac{\partial}{\partial x_2}$		1
$x_1^2 - x_2^2$	$2x_1 \dfrac{\partial}{\partial x_1} - 2x_2 \dfrac{\partial}{\partial x_2}$		1
$-x_1^2 - x_2^2$	$-2x_1 \dfrac{\partial}{\partial x_1} - 2x_2 \dfrac{\partial}{\partial x_2}$		2

Fig. 2.2 An example of critical points on a two-dimensional manifold called a torus $T^2 = S^1 \times S^1$ embedded in the three-dimensional Euclidean space. The Morse function is defined by the height function $f(p) = x_3$

sign of integral curves $\epsilon \colon \mathcal{M}(p, q) \to \{\pm 1\}$ according to cycles if they exist. In the example, if we set $\epsilon(\gamma_1) = 1$, then another should have opposite sign $\epsilon(\gamma_2) = -1$.

Let us define the Morse complex of index λ by the free $\mathbb{Z}$-module generated by all the critical points of index λ

$$C_\lambda := \bigoplus_{\lambda_i = \lambda} \mathbb{Z} p_i,$$

Fig. 2.3 Integral curves on the torus T^2 from critical points of index λ to ones of index $\lambda - 1$. There exist two curves from p_2 to p_0 that are not drawn
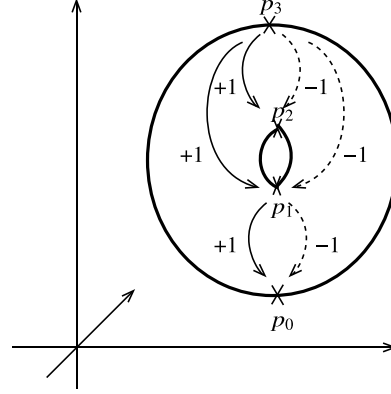
where λ_i denotes the index of the critical point p_i, and boundary operators $d_\lambda : C_\lambda \to C_{\lambda-1}$, which are homomorphisms, by

$$d_\lambda(p_i) := \sum_{\substack{\lambda_j = \lambda - 1 \\ \gamma \in \mathcal{M}(p_i, p_j)}} \epsilon(\gamma) p_j \quad \text{for all critical points } p_i \in C_\lambda.$$

Since we can see that $d_{\lambda-1} \circ d_\lambda = 0$, $(C_\bullet, d_\bullet)$ is a chain complex. The kth Morse homology group is defined by

$$H_k(M) := \operatorname{Ker} d_k / \operatorname{Im} d_{k+1}, \quad k = 0, 1, 2, \ldots.$$

For example, the Morse homology groups of the torus T^2 (Fig. 2.2) are computed as follows (see also Fig. 2.3): the Morse complexes are $C_0 = \mathbb{Z}p_0$, $C_1 = \mathbb{Z}p_1 \oplus \mathbb{Z}p_2$, $C_2 = \mathbb{Z}p_3$, and boundary operators are defined as $d_0(p_0) = 0$, $d_1(p_1) = (+1 - 1)p_0 = 0$, $d_1(p_2) = (+1 - 1)p_0 = 0$, $d_2(p_3) = (+1 - 1)p_1 + (+1 - 1)p_2 = 0$. Note that $C_k = 0$ for $k \geq 3$ and $k = -1$, and $d_k = 0$ for $k \geq 3$ and $k = 0$. Hence, $\operatorname{Ker} d_k = C_k$ and $\operatorname{Im} d_k = 0$ for all k, then we obtain $H_0(M) = C_0 \cong \mathbb{Z}$, $H_1(M) = C_1 \cong \mathbb{Z}^2$, and $H_2(M) = C_2 \cong \mathbb{Z}$. This example shows that the fewer critical points the Morse function has, the easier it is to compute the Morse homology.

One can find more details in, for example, Milnor's book [17].

2.2.3 Discrete Morse Theory

The discrete Morse theory is a combinatorial analog of the Morse theory developed by Forman [11, 12]. Although the discrete Morse theory is constructed on CW complexes abstractly in general, we explain the theory more concretely for simplicity.

We call the following k-dimensional cells, or simply k-cells:

- 0-cell: a point;
- 1-cell: a curve whose boundaries are points (0-cells);
- 2-cell: a surface whose boundaries are curves (1-cells);
- 3-cell: a solid whose boundaries are surfaces (2-cells);
- …

A set of cells $\mathcal{K}$ is called a cell complex if a k-cell α is included in $\mathcal{K}$ implies that all the boundaries of α are included in $\mathcal{K}$. A cell α is called a face of β if $\alpha \subset \beta$, where we consider a cell as a set of vertices. A face α of β is called maximal if $\dim \alpha = \dim \beta - 1$.

A function $f : \mathcal{K} \to \mathbb{R}$ is called a discrete Morse function if the following conditions are satisfied: for all $\alpha \in \mathcal{K}$,

1. $\#\{ \beta \in \mathcal{K} : \alpha \text{ is a maximal face of } \beta \text{ and } f(\alpha) \geq f(\beta) \} \leq 1$;
2. $\#\{ \gamma \in \mathcal{K} : \gamma \text{ is a maxima face of } \alpha \text{ and } f(\gamma) \geq f(\alpha) \} \leq 1$.

A cell $\alpha \in \mathcal{K}$ is called a critical cell if the following strict conditions are satisfied:

1. $\#\{ \beta \in \mathcal{K} : \alpha \text{ is a maximal face of } \beta \text{ and } f(\alpha) \geq f(\beta) \} = 0$;
2. $\#\{ \gamma \in \mathcal{K} : \gamma \text{ is a maximal face of } \alpha \text{ and } f(\gamma) \geq f(\alpha) \} = 0$.

For a non-critical cell $\alpha \in \mathcal{K}$, there exists a cell $\beta \in \mathcal{K}$, where α is a maximal face of β and $f(\alpha) \geq f(\beta)$, or $\gamma \in \mathcal{K}$, where γ is a maximal face of α and $f(\gamma) \geq f(\alpha)$. For these pairs of cells, we draw arrows from α to β or from γ to α. The set of these arrows is called a gradient vector field. For example, see Fig. 2.4.

Given a gradient vector field of a discrete Morse function f on $\mathcal{K}$, we call a sequence of k-cells α_i and $(k + 1)$-cells β_i alternately $(\alpha_1, \beta_1, \alpha_2, \beta_2, \ldots, \beta_r, \alpha_{r+1})$ a gradient path of f if, for each $i = 1, 2, \ldots, r$, a pair (α_i, β_i) is a vector of the gradient vector field, α_{i+1} is a face of β_i and $\alpha_{i+1} \neq \alpha_i$. By the definition, one can readily derive the relation $f(\alpha_1) \geq f(\beta_1) > f(\alpha_2) \geq f(\beta_2) > \cdots \geq f(\beta_r) > f(\alpha_{r+1})$. Then, we can obtain a way to compute the homology groups of $\mathcal{K}$ in a similar manner to the continuous Morse theory. Let C_λ be the Morse complex of dimension λ; i.e. C_λ
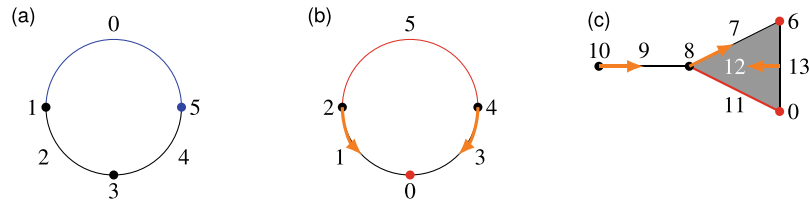

Fig. 2.4 Examples of cell complexes and discrete Morse functions. There are 0-cells (points), 1-cells (curves), and a 2-cell (surface; only in **c**), and numbers written next to each cell are the values of the discrete Morse functions. The function on **a** is not a discrete Morse function because blue cells do not satisfy the conditions. The functions on **b** and **c** are discrete Morse functions and red cells are critical cells. The orange arrows in **b** and **c** indicate a gradient vector fields
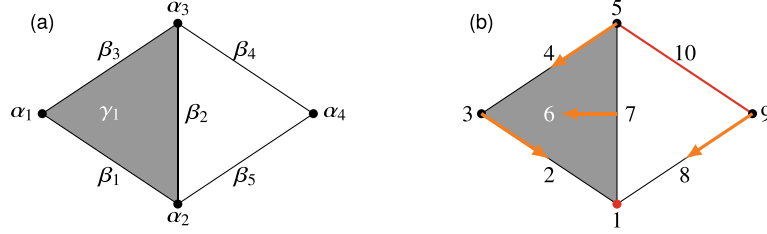
Fig. 2.5 An example of gradient paths and Morse homology groups. **a** indicates the names of the cells. **b** indicates the values of the discrete Morse function, the critical cells, and the gradient vector field

is the free $\mathbb{Z}$-module generated by all the critical λ-cells. Let $d_\lambda : C_\lambda \to C_{\lambda-1}$ be a boundary operator defined by

$$d_\lambda(\beta_i) := \sum_{\substack{\alpha_j:\text{critical }(\lambda-1)-cell \\ \gamma \in \mathcal{M}(\beta_i,\alpha_j)}} \epsilon(\gamma)\alpha_j \quad \text{for all critical cells } \beta_i \in C_\lambda,$$

where $\mathcal{M}(\beta_i, \alpha_j)$ is the set of all the gradient paths from a maximal face of β_i to the cell α_j, and $\epsilon(\gamma) \in \{\pm 1\}$ is determined depending on whether the chosen orientation on β_i induces the same orientation of the gradient path on α_j or the opposite orientation. Then, the Morse homology is defined by $H_k(\mathcal{K}) = \text{Ker } d_k/\text{Im } d_{k+1}$, $k = 0, 1, 2, \ldots$.

For example, consider the cell complex and the discrete Morse function in Fig. 2.5. There are a critical 0-cell α_2 and a critical 1-cell β_4, and gradient paths $(\alpha_4, \beta_5, \alpha_2)$ whose sign is $+1$ and $(\alpha_3, \beta_3, \alpha_1, \beta_1, \alpha_2)$ whose sign is -1. There are the complexes $C_0 = \mathbb{Z}\alpha_2$, $C_1 = \mathbb{Z}\beta_4$, $C_2 = 0$, and the boundary operators $d_0(\alpha_2) = 0$, $d_1(\beta_4) = (+1 - 1)\alpha_2 = 0, d_2 = 0$. Hence, Ker $d_k = C_k$ and Im $d_k = 0$ for all k, then we obtain $H_0(\mathcal{K}) = C_0 \cong \mathbb{Z}$, $H_1(\mathcal{K}) = C_1 \cong \mathbb{Z}$, and $H_2(\mathcal{K}) = 0$.

2.3 Application of Discrete Morse Theory to Traffic Flow Models

In this section, we consider an application of the discrete Morse theory, which was introduced in Sect. 2.2, to a simple traffic flow model called the Burgers cellular automaton.

2.3.1 Algorithms for Constructing Discrete Morse Functions on Cubical Complexes

To apply the discrete Morse theory, we first have to construct a complex and a discrete Morse function that possesses topological information of the data to be analyzed. We adapt the algorithms for constructing discrete Morse functions on cubical complexes to analyze 2D and 3D grayscale digital images proposed by Robins, Wood, and Sheppard [21]. The following is a brief exposition of the algorithm for 2D lattice. The algorithm for 3D lattice can be also described in the same manner.

Let us consider a discrete lattice

$$D = \{\, (i, j) \in \mathbb{Z}^2 : 0 \le i \le I, \ 0 \le j \le J \,\}.$$

We can derive a cubical complex $\mathcal{K}$ from the lattice D as follows: the vertices $(i, j) \in D$ are 0-cells of the complex $\mathcal{K}$. The unit edges between the vertices, and the unit squares are 1-cells and 2-cells of the complex $\mathcal{K}$, respectively.

Let $g : D \to \mathbb{R}$ be a function that represents a given numerical data on the lattice D. We assume that the vertices in D can be strictly totally ordered as $g(x_0) < g(x_1) < \cdots < g(x_N)$. Note that this requirement is always satisfied by adding perturbation to g without giving adverse effects to the results of the algorithm. Then, subsets of the neighboring cells of $x \in D$, called the lower stars of x,

$$L(x) = \{\, \alpha \in \mathcal{K} : x \in \alpha \text{ and } g(x) = \max_{y \in \alpha} g(y) \,\}$$

give a disjoint partition of $\mathcal{K}$:

$$\mathcal{K} = \bigsqcup_{x \in D} L(x).$$

The following algorithm works on each lower star $L(x)$ in parallel. As a preparation, for each k-cell $\alpha = \{x, y_1, \ldots, y_{2^k-1}\} \in L(x)$, define

$$G(\alpha) = \big(g(x), g(y_{i_1}), \ldots, g(y_{i_{2^k-1}})\big) \in \mathbb{R}^{2^k},$$

where $g(x) > g(y_{i_1}) > \cdots > g(y_{i_{2^k-1}})$, and list these vectors lexicographically.

1. If $L(x) = \{x\}$, then the 0-cell x is marked as critical and end. Otherwise, the 0-cell x is paired with the 1-cell $\delta \in L(x)$ that is minimal with respect to G ordering.
2. Add all other 1-cells in $L(x)$ to the priority queue `PQzero`, whose elements are ordered by G.
3. Add all cells $\alpha \in L(x)$ such that α is a face of δ and the number of its unpaired faces is exactly one to the priority queue `PQone`, whose elements are ordered by G.
4. Iterate the following procedure while the queue `PQone` is not empty:

   - Pop the top cell α in `PQone`.

- If there are no unpaired faces of α, then add α to the queue PQzero. Otherwise, the k-cell α is paired with a $(k + 1)$-cell β that is a single available unpaired face for the cell α. Remove the cell β from the queue PQzero and add all cells $\gamma \in L(x)$ such that γ is the face of both α and β and the number of its unpaired faces is exactly one to the queue PQone.

5. If the queue PQzero is empty, then end. Otherwise, pop the top cell γ in PQzero and mark γ as critical, add all cells $\alpha \in L(x)$ such that α is a face of γ and the number of its unpaired faces is exactly one to the queue PQone. Go to the step 4.

After executing the algorithm above for all the lower stars $L(x)$, all the cells in $\mathcal{K}$ are either marked as critical or paired with another cell. We can then define a discrete Morse function corresponding to g as follows. For each $x \in D$, if $L(x)$ has more than one cell, let δ be the 1-cell that is minimal with respect to G ordering. If $L(x)$ has $k > 2$ cells, let $\alpha_1, \alpha_2, \ldots, \alpha_{k-2}$ be the remaining cells in $L(x)$, which are ordered by when they are marked or paired, where if the cells α and β are paired and β is a face of α then β will immediately precede α. Let $\epsilon = \min_{x \neq y}\{|g(x) - g(y)|\}$, then a discrete Morse function $m \colon \mathcal{K} \to \mathbb{R}$ is defined by

$$
\begin{cases}
m(\delta) = g(x) - \dfrac{\epsilon}{10}, \\
m(x) = g(x), \\
m(\alpha_i) = g(x) + \dfrac{i\epsilon}{10}, \quad i = 1, 2, \ldots, k - 2.
\end{cases}
\tag{2.1}
$$

For this discrete Morse function, the pairings of cells yield its gradient vector field and the cells marked as critical become its critical cells.

Figure 2.6 illustrates examples of constructed discrete Morse functions and critical cells.

2.3.2 Application to Analysis of the Burgers Cellular Automaton

The Burgers cellular automaton [20] is a simple traffic flow model. Its time evolution equation is given by

$$
U_n^{(t+1)} = U_n^{(t)} + \min\left(C - U_n^{(t)}, U_{n-1}^{(t)}\right) - \min\left(C - U_{n+1}^{(t)}, U_n^{(t)}\right),
$$

where $n \in \mathbb{Z}$ denotes the site number, $t \in \mathbb{Z}$ is the discrete-time variable, and a positive constant $C \in \mathbb{Z}$ denotes the capacity of each site, i.e. $U_n^{(t)} \in \{0, 1, 2, \ldots, C\}$.

First, let us consider the case of $C = 1$:

$$
U_n^{(t+1)} = U_n^{(t)} + \min\left(1 - U_n^{(t)}, U_{n-1}^{(t)}\right) - \min\left(1 - U_{n+1}^{(t)}, U_n^{(t)}\right),
$$

(a)

$$\mathcal{K} \qquad L(g^{-1}(1)) \qquad L(g^{-1}(2)) \qquad L(g^{-1}(3)) \qquad L(g^{-1}(4))$$
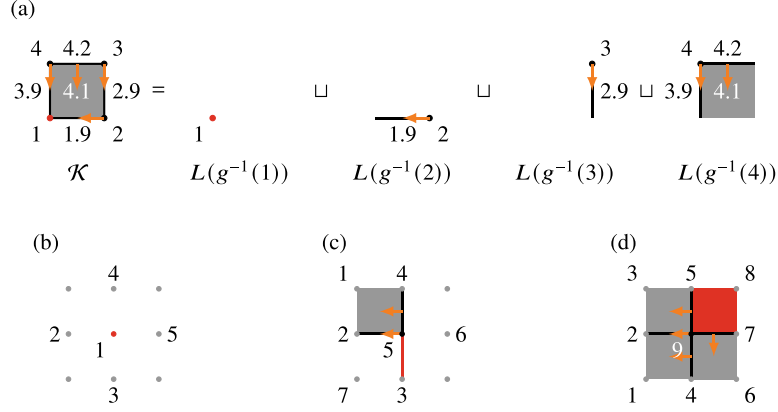
(b)   (c)   (d)

Fig. 2.6 Examples of constructed discrete Morse functions and critical cells. In each subfigure, numbers indicate the values of the original given functions or the constructed discrete Morse functions, orange arrows indicate the pairings of the cells in the algorithm or the gradient vector field, and red cells are critical, i.e. they have no paired cell. **a** The algorithm works on each lower star $L(x)$ in parallel. After pairing and marking, the values of a discrete Morse function are defined as equation (2.1). **b** An example of detecting a critical 0-cell, which is an analogue of a local minimum point in the continuous case. **c** An example of detecting a critical 1-cell, which is an analogue of a saddle point in the continuous case. **d** An example of detecting a critical 2-cell, which is an analogue of a local maximum point in the continuous case

which is also known as the elementary cellular automaton of rule 184 [27]. The value $U_n^{(t+1)}$ is determined by the values of 3-neighborhood $U_{n-1}^{(t)}$, $U_n^{(t)}$, and $U_{n+1}^{(t)}$:

$$\frac{U_{n-1}^{(t)}U_n^{(t)}U_{n+1}^{(t)}}{U_n^{(t+1)}} = \frac{111}{1}, \frac{110}{0}, \frac{101}{1}, \frac{100}{1}, \frac{011}{1}, \frac{010}{0}, \frac{001}{0}, \frac{000}{0}. \qquad (2.2)$$

Note that $10111000_2 = 184_{10}$. We impose the periodic boundary condition $U_{n+K}^{(t)} = U_n^{(t)}$ for all n and a positive constant $K \in \mathbb{Z}$. Let us define the particle density ρ by

$$\rho = \frac{1}{CK} \sum_{n=0}^{K-1} U_n^{(t)}.$$

Note that ρ is a conserved quantity of the Burgers cellular automaton. Figure 2.7a and b show examples of the time evolution of the Burgers cellular automaton with $\rho > 0.5$ and $\rho < 0.5$, respectively.

.

For the data $\{U_n^{(t)}\}_{t=0}^{T-1}$, we consider the function g defined by

$$g(n,t) = U_n^{(t)} + \frac{(K-n) + Kt}{20K(T-t)}, \qquad (2.3)$$
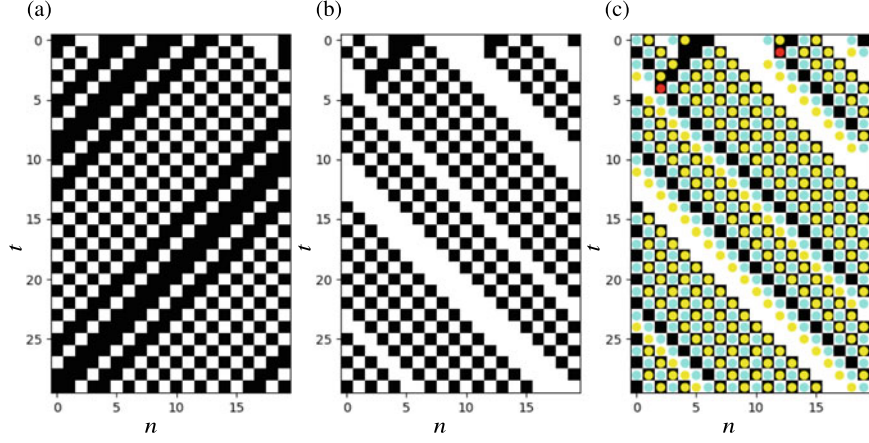
Fig. 2.7 Examples of the time evolution of the Burgers cellular automaton in the case of $C = 1$ and $K = 20$. White and black cells indicate $U_n^{(t)} = 0$ and 1, respectively. **a** In the case of $\rho > 0.5$, the steady state is a congested flow state. **b** In the case of $\rho < 0.5$, the steady state is a free flow state. **c** An example of applications of the discrete Morse theory to the states **b**. Blue, yellow, and red cells indicate that the lower star of the cell contains a critical 0-cell, a critical 1-cell, and a critical 2-cell, respectively

where the second term of the right-hand side is perturbation. Figure 2.7c shows an example of the result of the algorithm in the previous subsection for this function g. We can observe that critical 2-cells are detected at the points where a traffic jam disappears. This can be explained as follows. It is readily shown that the algorithm detects a critical 2-cell in a lower star $L(n, t)$ iff the value $g(n, t)$ is maximum in the Moore neighborhood of the point (n, t). In addition, under the definition (2.3),

- $g(\nu, \tau) < g(n, t)$ for $(\nu, \tau) = (n, t - 1), (n + 1, t - 1), (n + 1, t), (n + 1, t + 1)$
  iff $U_\nu^{(\tau)} \leq U_n^{(t)}$.
- $g(\nu, \tau) < g(n, t)$ for $(\nu, \tau) = (n - 1, t - 1), (n - 1, t), (n - 1, t + 1), (n, t + 1)$
  iff $U_\nu^{(\tau)} < U_n^{(t)}$.

Since $U_n^{(t)} \in \{0, 1\}$, the condition above implies that the lower star $L(n, t)$ contains a critical 2-cell iff

$$\begin{pmatrix} U_{n-1}^{(t-1)} & U_n^{(t-1)} & U_{n+1}^{(t-1)} \\ U_{n-1}^{(t)} & U_n^{(t)} & U_{n+1}^{(t)} \\ U_{n-1}^{(t+1)} & U_n^{(t+1)} & U_{n+1}^{(t+1)} \end{pmatrix} = \begin{pmatrix} 0 & * & * \\ 0 & 1 & * \\ 0 & 0 & * \end{pmatrix},$$

where $*$ allows either 0 or 1. However, from the time evolution rule of the Burgers cellular automaton (2.2), the $*$s above are uniquely determined as

$$\begin{pmatrix} U_{n-1}^{(t-1)} & U_n^{(t-1)} & U_{n+1}^{(t-1)} \\ U_{n-1}^{(t)} & U_n^{(t)} & U_{n+1}^{(t)} \\ U_{n-1}^{(t+1)} & U_n^{(t+1)} & U_{n+1}^{(t+1)} \end{pmatrix} = \begin{pmatrix} 0 & 1 & 1 \\ 0 & 1 & 0 \\ 0 & 0 & 1 \end{pmatrix}.$$
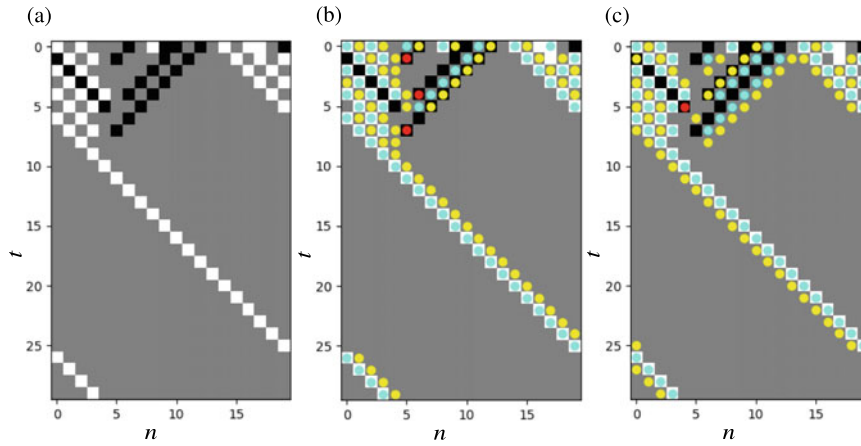
Fig. 2.8 **a** An example of the time evolution of the Burgers cellular automaton in the case of $C = 2$ and $K = 20$. White, gray, and black cells indicate $U_n^{(t)} = 0$, 1, and 2, respectively. **b** An example of applications of the discrete Morse theory to the states **a** using the function defined by (2.3). Blue, yellow, and red cells indicate that the lower star of the cell contains a critical 0-cell, a critical 1-cell, and a critical 2-cell, respectively. **c** An example using the function defined by (2.4) instead of (2.3). The meaning of color cells are same as in **b**

Therefore, a traffic jam disappears at the point (n, t) iff the lower star $L(n, t)$ contains a critical 2-cell.

For the case of $C = 2$, we can also show almost the same result in the same manner. See Fig. 2.8b. As another application, if we consider

$$g(n, t) = U_n^{(t)} + \frac{n + Kt}{20KT} \tag{2.4}$$

instead of (2.3), we can show in a similar manner that critical 2-cells are detected at the points where a free flow disappears. See Fig. 2.8c.

2.3.3 Application to Analysis of Pedestrian Flow

As a more practical application, we tried to apply the algorithm to the states of a pedestrian simulator developed by one of the authors, Zanlungo (see also Sect. 2.5). In the simulator, pedestrians are walking in a 2D map that has a crisscross corridor. Therefore the simulator generates $(2 + 1)$-dimensional (3D) data. From the data, we define a simple density function, pick its values on a lattice, construct the input function g with perturbation, and apply the algorithm for 3D lattice. Figure 2.9 shows an example of the result. At present, since this method detects a large number

Fig. 2.9 An example of
applications of the discrete
Morse theory to the states of
the pedestrian simulator by
Zanlungo. Yellow, blue,
green, and red cells indicate
that the lower star of the cell
contains a critical 0-cell, a
critical 1-cell, a critical
2-cell, and a critical 3-cell,
respectively
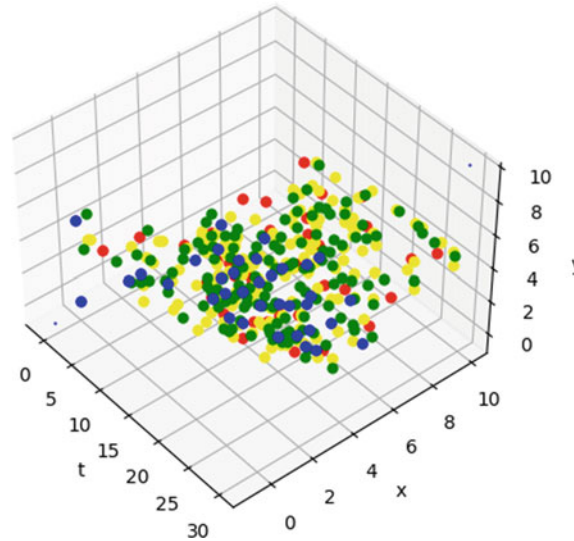
of critical cells, we are not able to interpret the result. It is left for future research to apply the discrete Morse theory not only to artificial simple data but also to practical data.

2.4 A Traffic Flow Model Using Quantum Walks

Quantum walk (QW), a quantum version of classical random walk, is widely applied to fast search algorithms by using quantum computers and modeling quantum systems [24]. Taking advantage of the flexibility of QWs, many extended QW models such as lattice models and many-particle models have been proposed [2, 24].

As discussed in the previous chapters, classical (non-quantum) particle models including cell automata have the potential to represent phenomena of traffic flow, and their properties have been studied for a long time. In real-world traffic flows, featured phenomena such as free running and congested phases and traffic vibration caused by repeated low-speed and high-speed states are known [16].

Although quantum computing has been widely applied to computational acceleration and modeling, quantum models have limited modeling of traffic flows. To investigate the applicability of quantum models to traffic flows, this section discusses how to construct a quantum model of traffic flows using QW, named one-way multi-particle quantum walks (OMQW). Also, by simulation, this section presents the behaviors of OMQW and displays the basic diagram of OMQW by using the "quantity of flow".

2.4.1 A Definition of One-Way Multi-particle Quantum Walks

In this part, we introduce n-particle discrete-time OMQW to discuss the quantum traffic flow model. Intuitively speaking, OMQW has two differences from standard discrete-time quantum walks. One is that it is composed of multiple particles (n particles), and the other is to introduce unidirectionality to express the flow. Several quantum models composed of many particles have already been reported, and OMQW now adopts the same approach as Costa et al to handle multiple particles [8]. They defined the interaction between particles by collision to consider the quantum version of gas model, i.e. collisions between particles occur if multiple particles arrive at the same coordinates as a result of movement. Their collision formulation is suitable for quantum models because it is unitary. Next, to realize unidirectionality, OMQW is a model which expands a quantum walk with two internal degrees of freedom, "move forward" and "stay". These two internal degrees of freedom are inspired by TASEP, where these two actions are selected stochastically. Contrastingly, OMQW treats them as states (of the coin) by means of quantum.

Before defining OMQW, we describe the definition of symbols related to OMQW. Let $\mathcal{H}_p$ be a Hilbert space and $\mathcal{H}_c$ be a finite dimensional Hilbert space. Let us denote an orthonormal basis in $\mathcal{H}_p$ by $\{|x\rangle\}_{x\in\mathbb{Z}}$, and an orthonormal basis in $\mathcal{H}_c$ by $\{|c\rangle\}_{c\in\{0,1\}}$. Then, an orthonormal basis of $\mathcal{H}_p \otimes \mathcal{H}_c$ can be written as $\{|x,c\rangle := |x\rangle \otimes |c\rangle\}_{x\in\mathbb{Z}, c\in\{0,1\}}$. By expanding these notation to n-particle, orthonormal set in $\hat{\mathcal{H}} := \bigotimes_{i=1}^{n}(\mathcal{H}_p \otimes \mathcal{H}_c)$ can be written as $\{|\boldsymbol{x},\boldsymbol{c}\rangle\}_{\boldsymbol{x}=(x_1,\ldots,x_n)\in\mathbb{Z}^n, \boldsymbol{c}=(c_1,\ldots,c_n)\in\{0,1\}^n}$.

OMQW is represented by operators on $\hat{\mathcal{H}}$, because the state transition of OMQW is identified by behaviors of n particles and n coins. More concretely, one step of OMQW consists of three operators: an n-particle collision operator $\hat{T}$, a shift operator $\hat{S}$, and coin operators $\hat{C}_{\boldsymbol{d}}$. The exact definitions of these three operators are a bit complicated, so the overall OMQW definition is described first, and then define these operators.

Definition 2.1 (*One-Way Multi-particle Quantum Walks*) If any states $|\psi_t\rangle \in \hat{\mathcal{H}}$ at time $t \in \mathbb{Z}_{\geq 1}$ satisfy the following conditions, we say that a dynamics of $|\psi_t\rangle$ is one-way multi-particle quantum walk (OMQW).

1. (Initial condition) The initial state $|\psi_0\rangle$ is given.
2. (Deterministic initial position) Let $\boldsymbol{s} \in \mathbb{Z}^n$ be initial position. For any $\boldsymbol{x} \in \mathbb{Z}^n$, $\boldsymbol{c} \in \{0,1\}^n$, if $\boldsymbol{x} \neq \boldsymbol{s}$, then $\|\langle \boldsymbol{x}, \boldsymbol{c}|\psi_0\rangle\|^2 = 0$ holds.
3. (State transition) The state transition is given by

$$|\psi_t\rangle = \sum_{\boldsymbol{d}\in\{0,1\}^n} \hat{T}\hat{S}\hat{C}_{\boldsymbol{d}}|\psi_{t-1}\rangle \tag{2.5}$$

In the rest of this section, we define these three operators consisting of OMQW and describe their properties.

2.4.1.1 Coin Operator

First of all, let us introduce a coin matrix for one particle $D \in U(2)$, where U means unitary group. We denote the i-th row j-th column element in D by $\alpha_{i,j} \in \mathbb{C}$. Note that the index of this matrix starts at zero, i.e. $i, j \in 0, 1$.

Let $d \in \{0, 1\}$ be an index representing the next state of a coin. A coin operator for a single particle $C_d : \mathcal{H}_p \otimes \mathcal{H}_c \to \mathcal{H}_p \otimes \mathcal{H}_c$ is defined as: $C_d := \sum_{\substack{x \in \mathbb{Z} \\ c \in \{0,1\}}} \alpha_{d,c} |x, d\rangle\langle x, c|$. Intuitively, this operation represents the change of the coin state from the current state c to the next state d.

The next definition describes the coin operator for multiple particles by extending the above coin operator for a single particle.

Definition 2.2 (*Coin operator*) For any $\boldsymbol{d} \in \{0, 1\}^n$, n-particle coin operator $\hat{C}_{\boldsymbol{d}} : \hat{\mathcal{H}} \to \hat{\mathcal{H}}$ is defined as:

$$\hat{C}_{\boldsymbol{d}} := \sum_{\substack{x_1,\dots,x_n \in \mathbb{Z} \\ c_1,\dots,c_n \in \{0,1\}}} \bigotimes_{i=1}^{n} (C_{d_i} |x_i, c_i\rangle\langle x_i, c_i|) \tag{2.6}$$

The following properties of the one-/n-particle coin operator hold.

- For any $\boldsymbol{d} \in \{0, 1\}^n$, $x \in \mathbb{Z}$, and $c \in \{0, 1\}$, the following equation holds:

$$C_d |x, c\rangle = \alpha_{d,c} |x, d\rangle \tag{2.7}$$

- For any $\boldsymbol{d} \in \{0, 1\}^n$, $\boldsymbol{x} \in \mathbb{Z}^n$, and $\boldsymbol{c} \in \{0, 1\}^n$, the following equation holds:

$$\hat{C}_{\boldsymbol{d}} |\boldsymbol{x}, \boldsymbol{c}\rangle = \bigotimes_{i=1}^{n} (C_{d_i} |x_i, c_i\rangle) = (\prod_{i=1}^{n} \alpha_{d_i,c_i}) |\boldsymbol{x}, \boldsymbol{c}\rangle \tag{2.8}$$

2.4.1.2 Shift Operator

The shift operator represents the one-time step movement of particles depending on the state of the coin.

Definition 2.3 (*Shift operator*) A one-particle shift operator $S : \mathcal{H}_p \otimes \mathcal{H}_c \to \mathcal{H}_p \otimes \mathcal{H}_c$ is defined as: $S := \sum_{\substack{x \in \mathbb{Z} \\ c \in \{0,1\}}} |x + c, c\rangle\langle x, c|$

An n-particle shift operator $\hat{S} : \hat{\mathcal{H}} \to \hat{\mathcal{H}}$ is defined as:

$$\hat{S} := \sum_{\substack{x_1,\dots,x_n \in \mathbb{Z} \\ c_1,\dots,c_n \in \{0,1\}}} \bigotimes_{i=1}^{n} (S |x_i, c_i\rangle\langle x_i, c_i|) \tag{2.9}$$

Then, the one-particle/n-particle shift operator satisfies the following two statements.

- For any $x \in \mathbb{Z}$ and $c \in \{0, 1\}$, the following equation holds: $S|x, c\rangle = |x + c, c\rangle$
- For any $\boldsymbol{x} = (x_1, \ldots, x_n) \in \mathbb{Z}^n$ and $\boldsymbol{c} = (c_1, \ldots, c_n) \in \{0, 1\}^n$, the following equation holds:

$$\hat{S}|\boldsymbol{x}, \boldsymbol{c}\rangle = \bigotimes_{i=1}^{n}(S|x_i, c_i\rangle) = |\boldsymbol{x} + \boldsymbol{c}, \boldsymbol{c}\rangle \tag{2.10}$$

2.4.1.3 Collision Operator

Before defining the collision operator, we introduce a collision function that represents whether a particle collides with another particle. Let $i \in \{1, \ldots, n\}$ be an index of particle. Collision function $r_i : \mathbb{Z}^n \times \{0, 1\} \rightarrow \{0, 1\}$ is defined as

$$r_i(\boldsymbol{x}, c) := \begin{cases} 1 - c & (\sum_{j=1}^{n} \delta_{x_i, x_j} \;\; is \;\; even) \\ c & (\sum_{j=1}^{n} \delta_{x_i, x_j} \;\; is \;\; odd) \end{cases} \tag{2.11}$$

where $\delta_{\cdot, \cdot}$ is Kronecker delta. By extending this function to n-particles, a collision function for n-particles $\hat{\boldsymbol{r}} : \mathbb{Z}^n \times \{0, 1\}^n \rightarrow \{0, 1\}^n$ is defined as

$$\hat{\boldsymbol{r}}(\boldsymbol{x}, \boldsymbol{c})_i := r_i(\boldsymbol{x}, c_i) \tag{2.12}$$

where $\hat{\boldsymbol{r}}(\boldsymbol{x}, \boldsymbol{c})_i$ is i-th element of $\hat{\boldsymbol{r}}(\boldsymbol{x}, \boldsymbol{c})$.

Definition 2.4 (*Collision operator*) n-particle collision operator $\hat{T} : \hat{\mathcal{H}} \rightarrow \hat{\mathcal{H}}$ is defined as

$$\hat{T} := \sum_{\substack{x_1, \ldots, x_n \in \mathbb{Z} \\ c_1, \ldots, c_n \in \{0, 1\}}} \bigotimes_{i=1}^{n}(|x_i, r_i(\boldsymbol{x}, c_i)\rangle\langle x_i, c_i|) \tag{2.13}$$

The collision operator describes the change of internal states ("move forward" and "stay") when particles collide. Typically, when two particles are at the same coordinates, the state of the particles is flipped.

The collision operator and function have the following properties:

- For $i \in \{1, \ldots, n\}$ and $\boldsymbol{x} \in \mathbb{Z}^n$, $r_i(\boldsymbol{x}, \cdot)$ is bijective.
- For $\boldsymbol{x} \in \mathbb{Z}^n$, $\hat{\boldsymbol{r}}(\boldsymbol{x}, \cdot)$ is bijective.
- For $\boldsymbol{x} \in \mathbb{Z}^n$, $\boldsymbol{c} \in \{0, 1\}^n$, applying a collision operator is represented as form:

$$\hat{T}|\boldsymbol{x}, \boldsymbol{c}\rangle = |\boldsymbol{x}, \hat{\boldsymbol{r}}(\boldsymbol{x}, \boldsymbol{c})\rangle \tag{2.14}$$

- For $x \in \mathbb{Z}^n$, and $c \in \{0, 1\}^n$, the following equation holds:

$$\hat{r}(x, \hat{r}(x, c)) = c \tag{2.15}$$

2.4.2 Probability Distribution of OMQW

When the positions of particles in OMQW are observed after t-step time evolution, the observation behaves stochastically due to their quantum nature. This quantum property of OMQW is derived from the standard single-particle one-dimensional QW. The standard QW does not have a property called locality, where probabilities concentrate at constant points as time goes to infinity, unlike classical random walks. In this section, to confirm the behavior related to the non-locality of OMQW experimentally, we describe the formulation of the probability distribution of positions of particles and a computational method of such a probability.

From the quantum nature, positions x and internal states c of particles are stochastically observed, and their joint probability at time t is described as follows: $\|\langle x, c | \psi_t \rangle\|^2$. Note that, by the definition related to deterministic initial positions of OMQW, observation at $t = 0$ should be observed at position s.

2.4.2.1 Computation of Probability

In this section, we derive a recursive formula to compute the probabilities of states of OMQW. To express the state on the computer specifically, coefficients of the state $a_{t,x,c} \in \mathbb{C}$ are introduced as $a_{t,x,c} := \langle x, c | \psi_t \rangle$. Since $\{|x, c\rangle\}_{x \in \mathbb{Z}^n, c \in \{0,1\}^n}$ is an orthonormal set on $\hat{\mathcal{H}}$, a state $|\psi_t\rangle$ can be represented as follows:

$$|\psi_t\rangle = \sum_{\substack{x \in \mathbb{Z}^n \\ c \in \{0,1\}^n}} a_{t,x,c} |x, c\rangle \tag{2.16}$$

By combining these coefficients with the definitions in the previous section, the following recursive formula with respect to $a_{t,x,c}$ can be deduced.

Theorem 2.1 (Recursive expression for $a_{t,x,c}$) *For any $t \in \mathbb{Z}_{\geq 1}$, $x \in \mathbb{Z}^n$, and $c \in \{0, 1\}^n$, the following equation holds:*

$$a_{t,x,c} = \sum_{\tilde{c} \in \{0,1\}^n} a_{t-1,x-\hat{r}(x,c),\tilde{c}} \left(\prod_{i=1}^{n} \alpha_{r_i(x,c_i),\tilde{c}_i} \right) \tag{2.17}$$

Note that, the reachable area from the initial position in t steps is limited by t. Let the reachable area be $R(t) \subset \mathbb{Z}^n$. If $x \in \mathbb{Z}^n \setminus R(t)$, then $a_{t,x,c} = 0$.
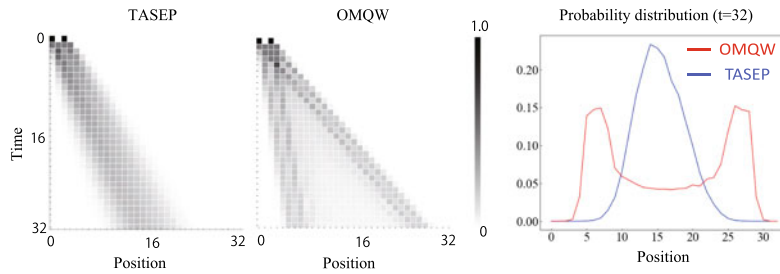
Fig. 2.10 This figure shows the time evolution of TASEP (left) and OMQW (center) where x-axis is position and y-axis is time step. Color intensity indicates the expected number of particles present at the position. The right figure shows the distributions of particles after 32 steps, these are corresponding with the bottom line of left and center figures
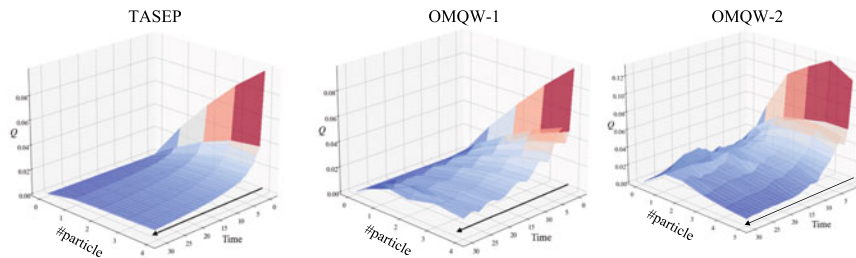

Fig. 2.11 Fundamental diagrams: quantity of flow related to the number of particles and time evolution for TASEP and OMQW (OMQW-1). OMQW-2 is experiments for an under periodic boundary conditions

This theorem can be proven by mathematical induction. By using this theorem, we can computationally simulate the state after any steps by performing recursively calculating with the above formula.

2.4.3 Simulation

This section carried out computer simulations on OMQW and TASEP using the definition until previous section (Fig. 2.10). These figures show the distributions of OMQW and TASEP, which are computed by simulation at 1000 times for each time step. The TASEP result shows a unimodal distribution related to the particle positions, whose center moves to the right. Contrastingly, the distribution of OMQW dividing into two modalities: slow and fast modal. A normal quantum walk is known to have two distribution peaks, which are the same as OMQW. A difference point is that OMQW constitutes a flow due to the introduction of unidirectionality.

Next, we introduce "quantity of flow" to discuss its properties as traffic flow. Let be position x and be time t. Quantity of flow Q_t is defined as

$$Q_t = 1/N \sum_0^{N-1} \max(E_{x,t} - E_{x,t-1}, 0)$$

where $E_{x,t}$ is expectation of the number of particles at time step t in OMQW, the initial position is set at random.

Figure 2.11 shows the relationship between this quantity, x, and t. Comparing the results of TASEP and those of OMQW, it can be seen that the quantity of flow of OMQW is oscillates related to time t. These properties, unlike classical models, might be used for modeling phenomena in traffic flow.

2.4.3.1 Summary

In this section, we discussed applicability of quantum walk to a traffic model. We introduced an OMQW model, which is an extension of QW to a traffic flow model. In the first experiment, we visualized the flow rate and clarified the basic properties of OMQW. In the future, we plan to take advantage of this property and extend it to a more realistic and applied model.

2.5 Pedestrian Flow and Future Perspectives

Understanding the dynamics of pedestrian crowds is of fundamental importance in a plethora of practical applications related to modern life, in particular in large urban areas, such as the planning of large-scale events, buildings, transportation hubs [14], or whole urban areas [3], both in normal and emergency situations (e.g. during natural disasters, fires, or even during pandemics [7]). While most of these applications focus on the macroscopic (large-scale) aspects of crowd dynamics, also the understanding of how pedestrians behave at the microscopic (individual) level has considerable practical relevance, in particular to the field of automatic navigation of cars, robots, and other vehicles in urban areas where pedestrians may be present or even dominant [23, 36], and to safety and surveillance [25]. Furthermore, improved understanding of microscopic behavior may reflect on the ability of reproducing macroscopic dynamics, as the latter may be strongly influenced by individual dynamics such as those determined by belonging to a social group [28, 30, 34, 35].

Along with the aforementioned practical relevance, crowd dynamics is also of extreme theoretical importance, as it may be described as a many-particle system (and, in the continuum limit, as a fluid) whose fundamental components are human beings, and thus represents a natural arena to try to apply the mathematical methods of statistical physics to social systems. Namely, while the relevant observables of

the problems are the same as in a classical physics system (density, fluid velocity, pressure at the macroscopic level, position velocity, acceleration, orientation at the microscopic level), the laws determining the dynamics are related to human behavior, with all the related challenges that this implies [13].

The understanding of crowd dynamics relies mainly on three related, but conceptually different, scientific challenges: (1) data collection, (2) modeling, and (3) data analysis. All three fields have seen considerable improvements in recent years. It is nowadays possible to detect and track pedestrian positions in real time, allowing to collect a large amount of information concerning pedestrian behavior in controlled [5] and "ecological" [26, 29] settings. These data have obviously inspired mathematical and computational models of pedestrian and crowd behavior, and allowed to calibrate such models [13].

In this project we are mainly interested in the third challenge, data analysis. Pedestrian flow presents obviously many common points with the vehicular flow, analyzed in Sect. 2.3, but it is inherently more complex than the former. By being less strictly regulated than vehicular traffic, and composed of basic units (pedestrians) whose motion is less dynamically constrained than that of cars, pedestrian flow is a completely 2-dimensional phenomenon, while vehicular flow presents strong 1-dimensional features, and thus its topological properties are more complex.

As a result, practical and theoretical applications of discrete Morse theory to pedestrian flows are expected to be developed only after the relevant vehicular ones, and for this reason in the present section, we necessarily report a research plan more than actual accomplishments. Nevertheless, we believe that the contribution of the proposed framework to the study of crowd dynamics and pedestrian behavior may be extremely relevant and promising.

While as stated above the pedestrian flow problem is inherently 2-dimensional, most literature works focus on simplified settings that basically reduce it to a 1-dimensional one, such as corridors or bottlenecks [1, 9, 10, 19, 22, 37], and as a result also the related analysis tools are based on observables that do not rely on the 2-dimensional structure of space, such as pedestrian density and average speed.

On the other hand, a recent work [31] has introduced a novel metric, congestion number CN, to assess the state of a pedestrian crowd. This metric, being based on the magnitude of the gradient of the only non-zero component (i.e. normal to the floor) of the rotor of the pedestrian velocity

$$\|\nabla (\nabla \times \mathbf{v})_z\| \tag{2.18}$$

(divided by a theoretical reference value to obtain a pure number), is more apt to study actual 2-dimensional phenomena, and has proved to provide additional information with respect to the traditional 1-dimensional tools.

The aforementioned theoretical tool has been applied also to a geometrical setting that, although being still extremely simple if compared to the complexity of the real world, is fully two-dimensional, namely the cross-flow problem, i.e. the dynamics of two different pedestrian streams crossing at a non-trivial angle $\theta \neq n\pi$ ($\theta = n\pi$ corresponding to the well-studied corridor case).

This problem, and in particular the related formation of self-organized patterns (stripes) in the crossing area, has been the object of a few recent contributions, focusing on how the dynamics are affected by the angle θ [18] and by pedestrian density [32], on the ability of different collision avoidance models to reproduce the observed dynamics [33], and on a mathematical model of the self-organization phenomenon [4].

We believe the cross-flow scenario to be a benchmark to test the potential of the discrete Morse theory in studying flow properties that go beyond the vehicular applications analyzed in Sect. 2.3. We first of all aim to develop a way to use the discrete Morse theory to identify criticalities in the cross-flow scenario that may go beyond an analysis based only on density and speed, in a way similar to the results achieved by [31].

After this first goal is achieved, the method may be applied to still poorly understood phenomena. The ultimate challenge is to apply the method to the study of real-world data, possibly to understand which geometrical settings and crowd conditions may lead to dangerous circumstances and possibly to casualties.

While this is an extremely difficult task, an intermediate goal may be to study more complex versions of the basic cross-flow scenario, i.e. by increasing the number of flows or introducing obstacles [6].

While, as stated above, this project is aimed at tackling the challenge of "data analysis", such a task cannot be independent of data collection and modeling. We will use and further develop the computational models of [33] to obtain artificial data that may be used to test the proposed discrete Morse theory-based analysis on different crowd settings.

Obviously, while artificial data have the merit of being easily and safely produced and analyzed, data concerning actual pedestrian behavior are indispensable to develop an analysis tool that aims to describe the real world. While in this project we will mainly rely on the increasing number of freely available data concerning controlled experiments and real-world behavior, we do not discard the possibility of performing some simple experiments with human participants explicitly aimed at the development of the proposed analysis methods.

References

1. J. Adrian, A. Seyfried, A. Sieben, Crowds in front of bottlenecks at entrances from the perspective of physics and social psychology. J. R. Soc. Interface **17**(165), 20190871 (2020)
2. A. Ahlbrecht, A. Alberti, D. Meschede, V.B. Scholz, A.H. Werner, R.F. Werner, Molecular binding in interacting quantum walks. New J. Phys. **14**(7), 073050 (2012)
3. S.M. Arisona, G. Aschwanden, J. Halatsch, P. Wonka, *Digital Urban Modeling and Simulation* (Springer, 2012)
4. K.A. Bacik, B.S. Bacik, T. Rogers, Lane nucleation in complex active flows. Science **379**(6635), 923–928 (2023)
5. M. Boltes, A. Seyfried, Collecting pedestrian trajectories. Neurocomputing **100**, 127–133 (2013)

6. S. Cao, A. Seyfried, J. Zhang, S. Holl, W. Song, Fundamental diagrams for multidirectional pedestrian flows. J. Stat. Mech.: Theory Exp. **2017**(3), 033404 (2017)
7. S. Comai, S. Costa, S.M. Mastrolembo Ventura, G. Vassena, L. Tagliabue, D. Simeone, E. Bertuzzi, G. Scurati, F. Ferrise, A. Ciribini, Indoor mobile mapping system and crowd simulation to support school reopening because of COVID-19: a case study, in *Proceedings of the 13th GeoInformation for Disaster Management Conference* (2020), pp. 29–36
8. P.C. Costa, F. De Melo, R. Portugal, Multiparticle quantum walk with a gas like interaction. Phys. Rev. A **100**(4), 042320 (2019)
9. C. Feliciani, K. Nishinari, Empirical analysis of the lane formation process in bidirectional pedestrian flow. Phys. Rev. E **94**(3), 032304 (2016)
10. C. Feliciani, I. Zuriguel, A. Garcimartín, D. Maza, K. Nishinari, Systematic experimental investigation of the obstacle effect during non-competitive and extremely competitive evacuations. Sci. Rep. **10**(1), 1–20 (2020)
11. R. Forman, Morse theory for cell complexes. Adv. Math. **134**, 90–145 (1998)
12. R. Forman, A user's guide to discrete morse theory. Sémin. Lothar. Comb. **48**, B48c (2002)
13. D. Helbing, P. Molnar, Social force model for pedestrian dynamics. Phys. Rev. E **51**(5), 4282 (1995)
14. G. Hoy, E. Morrow, A. Shalaby, Use of agent-based crowd simulation to investigate the performance of large-scale intermodal facilities: case study of union station in Toronto, Ontario. Canada. Transp. Res. Rec. **2540**(1), 20–29 (2016)
15. T. Kaczynski, K. Mischaikow, M. Mrozek, *Computational Homology* (Springer, 2004)
16. X. Li, F. Peng, Y. Ouyang, Measurement and estimation of traffic oscillation properties. Transp. Res. Part B: Methodol. **44**(1), 1–14 (2010)
17. J. Milnor, Morse theory. Ann. Math. **51** (1963)
18. P. Mullick, S. Fontaine, C. Appert-Rolland, A.-H. Olivier, W.H. Warren, J. Pettré, Analysis of emergent patterns in crossing flows of pedestrians reveals an invariant of "stripe" formation in human data. PLOS Comput. Biol. **18**(6), e1010210 (2022)
19. H. Murakami, C. Feliciani, Y. Nishiyama, K. Nishinari, Mutual anticipation can contribute to self-organization in human crowds. Sci. Adv. **7**(12), eabe7758 (2021)
20. K. Nishinari, D. Takahashi, Analytical properties of ultradiscrete Burgers equation and rule-184 cellular automaton. J. Phys. A: Math. Gen. **31**, 5439–5450 (1998)
21. V. Robins, P.J. Wood, A.P. Sheppard, Theory and algorithms for constructing discrete morse complexes from grayscale digital images. IEEE Trans. Pattern Anal. Mach. Intell. **33**(7), 1646–1658 (2011)
22. A. Seyfried, O. Passon, B. Steffen, M. Boltes, T. Rupprecht, W. Klingsch, New insights into pedestrian flow through bottlenecks. Transp. Sci. **43**(3), 395–406 (2009)
23. M. Shiomi, F. Zanlungo, K. Hayashi, T. Kanda, Towards a socially acceptable collision avoidance for a mobile robot navigating among pedestrians using a pedestrian model. Int. J. Robot. Res. **6**(3), 443–455 (2014)
24. S.E. Venegas-Andraca, Quantum walks: a comprehensive review. Quantum Inf. Process. **11**(5), 1015–1106 (2012)
25. X. Wang, M. Wang, W. Li, Scene-specific pedestrian detection for static video surveillance. IEEE Trans. Pattern Anal. Mach. Intell. **36**(2), 361–374 (2013)
26. J. Willems, A. Corbetta, V. Menkovski, F. Toschi, Pedestrian orientation dynamics from high-fidelity measurements. Sci. Rep. **10**(1), 1–10 (2020)
27. S. Wolfram, Computation theory of cellular automata. Commun. Math. Phys. **96**, 15–57 (1984)
28. Z. Yücel, F. Zanlungo, M. Shiomi, Modeling the impact of interaction on pedestrian group motion. Adv. Robot **32**(3), 137–147 (2018)
29. F. Zanlungo, D. Brščić, T. Kanda, Spatial-size scaling of pedestrian groups under growing density conditions. Phys. Rev. E **91**(6), 062810 (2015)
30. F. Zanlungo, L. Crociani, Z. Yücel, T. Kanda, The effect of social groups on the dynamics of bi-directional pedestrian flow: a numerical study. Traffic Granul. Flow **2019**, 307–313 (2020)
31. F. Zanlungo, C. Feliciani, Z. Yücel, X. Jia, K. Nishinari, T. Kanda, A pure number to assess "congestion" in pedestrian crowds. Transp. Res. Part C: Emerg. Technol. **148**, 104041 (2023)

32. F. Zanlungo, C. Feliciani, Z. Yücel, K. Nishinari, T. Kanda, Macroscopic and microscopic dynamics of a pedestrian cross-flow: Part I, experimental analysis. Saf. Sci. **158**, 105953 (2023)
33. F. Zanlungo, C. Feliciani, Z. Yücel, K. Nishinari, T. Kanda, Macroscopic and microscopic dynamics of a pedestrian cross-flow: Part II, modelling. Saf. Sci. **158**, 105969 (2023)
34. F. Zanlungo, T. Ikeda, T. Kanda, Potential for the dynamics of pedestrians in a socially interacting group. Phys. Rev. E **89**(1), 012811 (2014)
35. F. Zanlungo, Z. Yücel, D. Brščić, T. Kanda, N. Hagita, Intrinsic group behaviour: dependence of pedestrian dyad dynamics on principal social and personal features. PLOS ONE **12**(11), e0187253 (2017)
36. F. Zanlungo, Z. Yücel, F. Ferreri, J. Even, L.Y. Morales Saiki, T. Kanda, Social group motion in robots, in *Proceedings of the 9th International Conference on Social Robotics* (2017), pp. 474–484
37. J. Zhang, W. Klingsch, A. Schadschneider, A. Seyfried, Ordering in bidirectional pedestrian flows and its influence on the fundamental diagram. J. Stat. Mech.: Theory Exp. **2012**(02), P02002 (2012)